Aalborg Universitet

Wave power absorption by a submerged balloon fixed to the sea bed

Kurniawan, Adi; Greaves, Deborah

Link to publication from Aalborg University

Wave power absorption by a submerged balloon fixed to the sea bed

Adi Kurniawan[1] ✉, Deborah Greaves[2]

[1]*Department of Civil Engineering, Aalborg University, Aalborg, Denmark*
[2]*School of Marine Science and Engineering, Plymouth University, Plymouth, UK*
✉ *E-mail: aku@civil.aau.dk*

Abstract: The possibility of absorbing wave energy using a submerged balloon fixed to the sea bed is investigated. The balloon is in the form of a fabric encased within an array of meridional tendons which terminate at a point at the top of the balloon and at some radius at the bottom. The expansion and contraction of the balloon in waves pump air via a turbine into and out of a chamber of constant volume. A more refined model than that used by Kurniawan and Greaves [*Proc. Second Offshore Energy and Storage Symp.*, 2015] predicts a similarly broad-banded response, but the maximum absorption is less than previously predicted. Both approaches are compared and discussed.

1 Introduction

To optimally absorb energy from ocean waves, it is well known that a wave energy device needs to oscillate with optimum amplitude and phase [1, 2]. The period and amplitude of ocean waves are however never constant, but varying at all time scales. The device needs to operate as close as possible to the two optimum conditions not just for a single wave amplitude and a single wave period, but for a range of wave amplitudes and periods, typically from 5 to 15 s. This challenge is particularly pertinent for point absorbers, which by definition are much smaller than the incident wavelengths [3]. A conventional rigid-bodied point absorber has an inherently narrow resonance bandwidth and without any phase control is not able to capture a significant portion of energy available beyond its natural period.
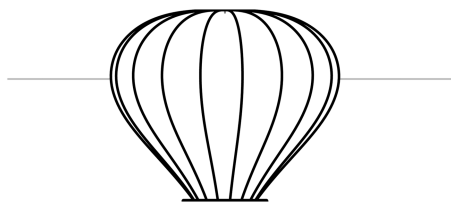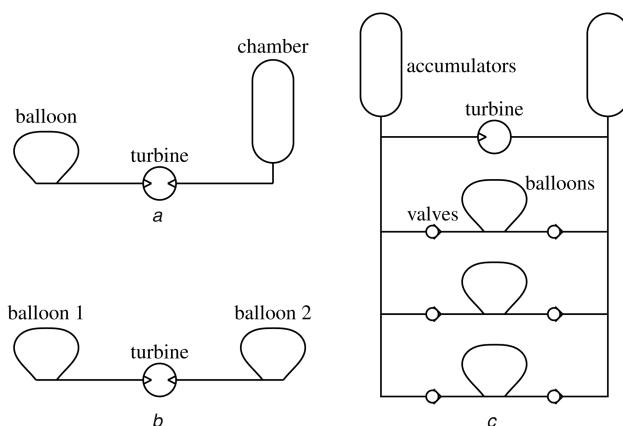

Fig. 1 *Sketch of the balloon*

Fig. 2 *Device schematics*
(a) Solo device, *(b)* Device in tandem, *(c)* Device in array

A recent study has however suggested that a point absorber in the form of a bottom-mounted vertical cylinder whose top is free to oscillate vertically can have an extremely broad-banded power absorption, even in the absence of any phase control [4]. Motivated by this, we considered a conceptually similar device, but with a completely flexible balloon replacing the cylinder, with the aim of reducing cost even more [5].

The balloon is of the same type as the underwater balloon used in [6] as a compressed air energy storage. The construction is that of a fabric encased within an array of meridional tendons which terminate at a point at the top of the balloon and at some radius at the bottom (see Fig. 1). In the simplest configuration, a single balloon is connected to a chamber of constant volume via a self-rectifying air turbine (Fig. 2a). As the balloon expands and contracts under wave action, air is exchanged with the chamber, driving the turbine. The chamber is not required if two balloons are spaced at approximately half a wavelength apart (Fig. 2b). With an array of balloons (Fig. 2c), it may be more cost-effective to have two centralised accumulators and a single common turbine, with a system of check valves directing air flow from the balloons through the turbine and back to the balloons. As the balloons are fixed to the sea bed, they are suited for nearshore locations with water depths of about 10 m. One or two rows of balloons aligned perpendicular to the incident wave direction will act at the same time as breakwaters [7].

In this paper, the response of the device in the simplest configuration (Fig. 2a) will be predicted numerically. The shape of the balloon is defined by the profile of its tendons, and therefore the challenge is in predicting how the tendons will move when the balloon is subjected to waves. Previously, this was done by predefining a mode shape to describe the deformation of the tendons [5]. The mode shape was taken as the difference between the static profile of the tendons at the mean pressure and that at a slightly different pressure. Such approach predicted a broad-banded response whose magnitudes were almost proportional to the volume of the chamber.

The purpose of this paper is to extend the previous analysis to allow the tendons to deform more naturally without any a priori assumption on the mode of deformation. Both the previous and the present approaches rely on the prediction of the static behaviour of the balloon in still water, and this will be first examined. As in the previous approach, we assume small wave amplitudes and small deformations of the balloon to justify the use of linear potential theory to obtain the hydrodynamic forces on the balloon and the use of linearised isentropic relations for an ideal gas to obtain the
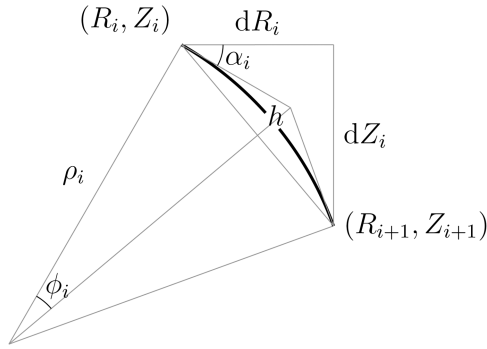
Fig. 3 *One discretised tendon element of length h. The radius R_i is measured from the vertical axis of the balloon. The elevation Z_i is measured from the water line*

pneumatic forces. Furthermore, the turbine is modelled as a linear resistance.

2 Static behaviour

When the balloon is inflated, the fabric forms meridional lobes between the tendons, keeping the tension in the fabric to a minimum while the tendons carry most of the tension. When the internal–external pressure difference is uniform, the balloon assumes an isotensoid shape, which was first derived by Taylor in his studies of parachutes [8]. Submerged in water, however, the shape of the balloon is more like an inverted and truncated pear, due to the increasing hydrostatic pressure with depth.

Since the balloon is axisymmetric, the shape of the balloon is defined by the profile of just a single tendon. To obtain the profile of the tendon, we start off by discretising the tendon into N arc elements having identical lengths h, but unknown radii of curvature ρ_i. One such element is shown in Fig. 3. The arc length h is related to the radius of curvature ρ_i through

$$h = -2\rho_i \phi_i, \qquad (1)$$

where $2\phi_i = \mathrm{d}\alpha_i$ is the arc sector angle in radians. Similarly, the distances $\mathrm{d}R_i$ and $\mathrm{d}Z_i$ can be expressed in terms of h, ϕ_i, and α_i.

The radius ρ_i of each element is obtained by solving the force equilibrium normal to the element, according to

$$\rho_i = \frac{T}{2\pi P_{i+0.5} R_{i+0.5}}, \qquad (2)$$

where T is the sum of tension in all tendons, while $P_{i+0.5}$ and $R_{i+0.5}$ are the internal–external pressure difference at the midpoint of element i and the distance from the vertical axis of the balloon to the same point. If the midpoint is above water, then $P_{i+0.5} = P$, which is the uniform internal pressure above atmospheric. If the midpoint is under water, then $P_{i+0.5} = P + \rho g Z_{i+0.5}$, where the last term is the external (hydrostatic) pressure.

The calculation starts at the top of the balloon, where $R_1 = \alpha_1 = 0$, and proceeds piecewise downwards along the tendon. The top elevation of the balloon Z_1 and the tendon tension T are not known beforehand, so an iterative procedure is necessary to obtain the correct Z_1 and T to give the correct radius and elevation at the bottom of the balloon. This means repeating the calculation with different Z_1 and T until the differences between (R_{N+1}, Z_{N+1}) and the specified $(R_{\mathrm{bot}}, Z_{\mathrm{bot}})$ are less than some small tolerances.

This method of calculating the shape of the balloon assumes that the tendons are inextensible and that all forces are transferred to the tendons. This is equivalent in theory to a balloon with infinitely many tendons. Nevertheless, the calculated profiles have been shown to be in good agreement with the actual profiles of a scaled model balloon having 16 tendons. Further details were given in [9].
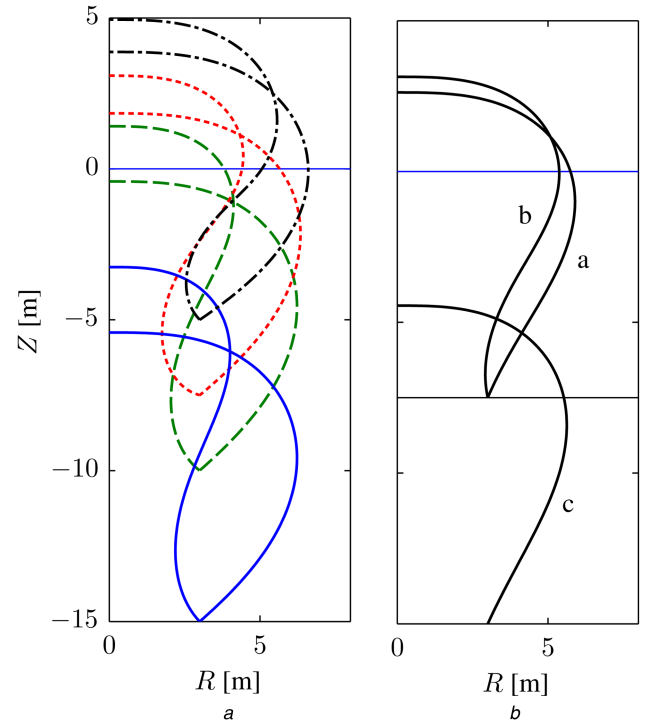

Fig. 4 *Calculated tendon profiles of a balloon with 15-m tendon length and 3-m bottom radius*
(a) Calculated tendon profiles for various bottom submergences: 15, 10, 7.5, and 5 m, Two profiles are shown for each bottom elevation, corresponding to the minimum and maximum pressures used in Fig. 5, *(b)* Equilibrium tendon profiles for cases specified in Table 1

In this paper, the length of one tendon from the top to the bottom of the balloon is chosen to be 15 m, and the bottom radius 3 m. The bottom radius needs to be sufficiently large to minimise pitching of the balloon in waves. The consequence however is that there will be a hoop load at the base as well as a requirement for a pulling-down load. It would be more attractive from practical point of view if the tendons came to a point at the base.

The calculated tendon profiles of this balloon with 15-m tendon length and 3-m bottom radius are shown in Fig. 4a, for various bottom elevations. When the balloon is completely underwater, the external pressure in the static case varies linearly with depth. Hence, the tendon profile of a balloon with its bottom submerged a m below the water level is exactly the same as that of a balloon submerged $a+b$ m below the water level, provided its internal pressure is increased by b m of water. This is evident from Fig. 4a: the profile of the balloon with its bottom submerged 15 m below the water level and with 18 m internal pressure (outer solid line) is the same as that of the balloon which sits 5 m higher and with its internal pressure reduced to 13 m (outer dashed line). On the other hand, when the balloon is partly submerged or surface-piercing, the external pressure below the water level varies linearly with depth, while above the water it is uniform. The variation of the internal–external pressure difference from the top to the bottom of a surface-piercing balloon is therefore unique for each bottom submergence, resulting in a unique profile for each combination of internal pressure and bottom submergence.

When the internal pressure (in metres of water) is less than the bottom submergence of the balloon, the tendon curvature is reversed at a depth equal to the internal pressure. The internal–external pressure difference is zero at this inflection point. Above this point, the internal pressure is higher than the external pressure, while below it, the internal pressure is lower than the external pressure. Thus, above and below this point, the tendon is bulging outward and inward, respectively.

In Fig. 5, various static parameters of the balloon are plotted as functions of the internal pressure and bottom submergence of the balloon. The top of the balloon generally rises as the internal pressure decreases, except at the lowest pressures, where the top of the balloon falls slightly due to the increased curvature of the
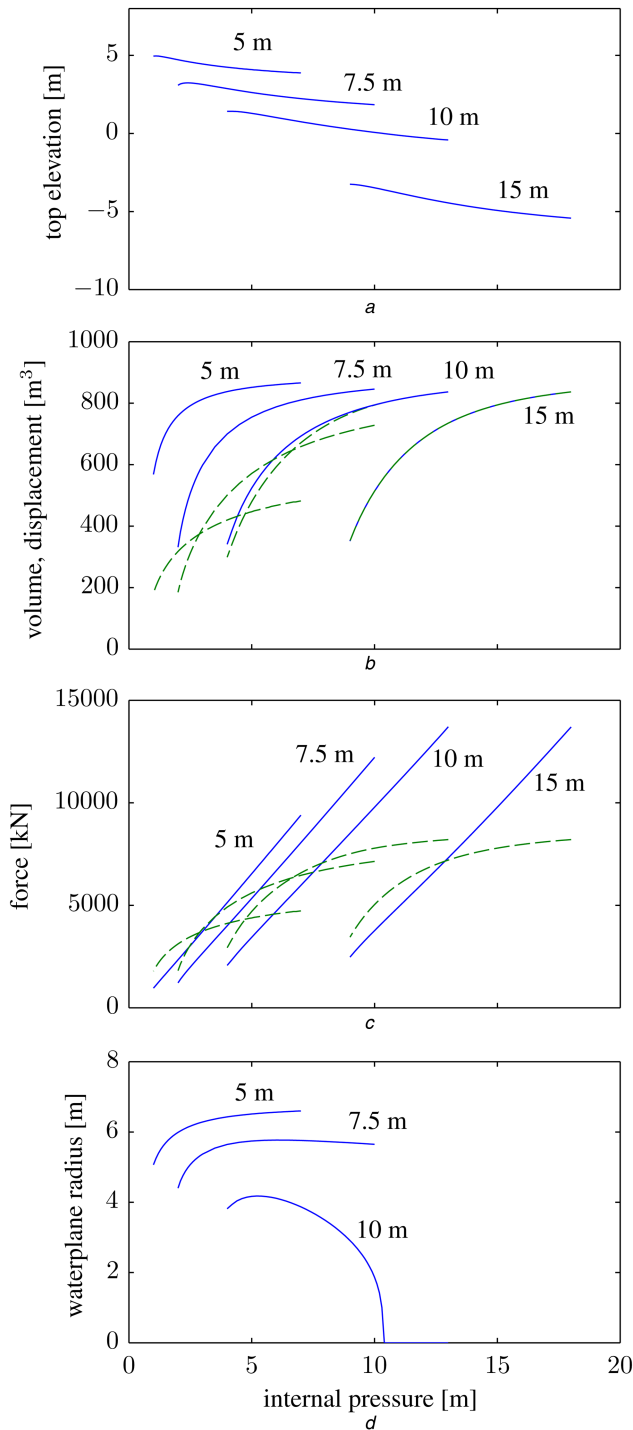
Fig. 5 *Variations of static parameters of the balloon with internal pressure, for various bottom submergences*
(a) Top elevation, *(b)* Volume (solid) and displacement (dashed), *(c)* Sum of tension in all tendons (solid) and upward force on the base (dashed), *(d)* Waterplane radius.

Table 1 Water depths, mean pressures, and calculated equilibrium volumes and surface areas of the balloon in cases a–c

Case	Water depth, m	Mean pressure, m	Mean volume, m^3	Mean surface area, m^2
a	7.5	5	754	384
b	7.5	3	598	341
c	15	13	735	375

tendon as the point of inflection rises with decreasing pressure (Fig. 5*a*). The volume of the balloon increases with the internal pressure at a decreasing rate, where the volume of the balloon

hardly increases at high pressures (Fig. 5*b*). Since there is not much change in volume when the internal pressure (in metres of water) is higher than the bottom submergence of the balloon, the operating mean pressure of the balloon should probably be lower than its bottom submergence.

From Fig. 5*c*, we see that the tension in the tendons varies approximately linearly with pressure, which is quite remarkable, while the upward force on the base is proportional to the displacement of the balloon. The variation of the waterplane radius of the balloon with pressure is more subtle (Fig. 5*d*). For a balloon with a relatively low bottom submergence, the waterplane radius appears to increase monotonically with pressure. With a deeper bottom submergence, the waterplane radius first increases and then decreases with increasing pressure. The waterplane radius decreases more quickly with pressure as the bottom submergence gets deeper.

3 Dynamic response

The cases specified in Table 1 will be considered. The corresponding mean tendon profiles are shown in Fig. 4*b*. The balloon is assumed to sit exactly on the sea bed. Thus, the water depth specified in Table 1 also indicates the bottom submergence of the balloon. The balloons are assumed to be completely axisymmetric, with the lobes neglected, and only axisymmetric deformations will be considered.

The difference between the previous approach [5] and the present one lies in the modelling of the deformation of the tendons, but the pneumatic aspects are the same. For both approaches, linearised isentropic relations for an ideal gas are used to model the air pressure–density relationship in the balloon and in the chamber, and the flow through the turbine is assumed to follow a linear relationship. Then, it can be shown [4] that the pressure p_c and volume amplitude v_c of the bag are related through

$$v_c = -V_c\left(\frac{M_f}{M_c}G + \frac{1}{\gamma(P + P_{atm})}\right)p_c \equiv -p_c/E, \qquad (3)$$

with

$$G = \frac{C}{\gamma(P + P_{atm})C + i\omega M_f}. \qquad (4)$$

Here, P is the mean internal pressure (which excludes the atmospheric pressure P_{atm}), $\gamma = 1.4$ is the heat capacity ratio, p_f and m_f are the complex amplitudes of the pressure and mass of air in the chamber, M_f is the mean air mass in the chamber, v_c, m_c, and p_c are the complex amplitudes of the volume, mass, and pressure of air in the balloon, while V_c and M_c are the mean volume and mass of air in the balloon. The mass flow through the turbine for a unit pressure difference is defined as the turbine coefficient C.

The mean absorbed power can finally be obtained from

$$\mathcal{P} = \frac{C}{2\rho_{air}}|p_c - p_f|^2 \qquad (5)$$

Once the deformation of the tendons is known, by which we can calculate the pressure amplitudes p_c and p_f.

3.1 Previous approach

In the previous approach [5], the tendons were assumed to deform according to a predefined mode whose shape was obtained from the difference between the static tendon profile at the mean pressure and a static profile obtained at a slightly different pressure. The hydrodynamic coefficients (wave excitation force, added mass, and radiation damping) associated with the mode of deformation of the balloon were computed using a three-dimensional (3D) panel method [10] by specifying either the normal or the Cartesian components of the mode shape over the balloon's mean wetted surface.

Since there was only one degree of freedom in total, the complex velocity amplitude U of the balloon was obtained by solving the following equation of motion:

$$\left[i\omega(M+m)+(B+B_\text{p})+\frac{1}{i\omega}(K+K_\text{p})\right]U=F_\text{e},\qquad(6)$$

where M is the generalised mass excluding the added mass, m is the added mass, B is the radiation damping, K is the hydrostatic stiffness, F_e is the wave excitation force, while B_p and K_p are the pneumatic damping and stiffness. The generalised mass M was expressed in terms of an integral over the mean volume of the balloon

$$M=\iiint_V \rho_\text{m}\boldsymbol{S}\cdot\boldsymbol{S}\,\mathrm{d}V,\qquad(7)$$

where $\rho_\text{m}(\boldsymbol{x})$ is the density of the balloon. The mode shape $\boldsymbol{S}(\boldsymbol{x})$, where $\boldsymbol{x}=(X,Y,Z)$ is the coordinates of any point on the balloon, was written in Cartesian components as

$$\begin{aligned}\boldsymbol{S}(\boldsymbol{x})&=(u(\boldsymbol{x}),v(\boldsymbol{x}),w(\boldsymbol{x}))^\text{T}\\&=(r_\text{a}(\overline{Z})\cos\theta,r_\text{a}(\overline{Z})\sin\theta,z_\text{a}(\overline{Z}))^\text{T},\end{aligned}\qquad(8)$$

where $r_\text{a}(\overline{Z})$ and $z_\text{a}(\overline{Z})$ are the radial and vertical components of the assumed mode shape, expressed as functions of a vertical coordinate normalised such that its value is equal to zero at the bottom of the bag and one at the top, and θ is the azimuthal angle. Similarly, the hydrostatic stiffness K was expressed in terms of an integral over the mean wetted body surface, following [11]:

$$K=\rho g\iint_{S_\text{b}} n(w+ZD)\mathrm{d}S,\qquad(9)$$

where ρ is the water density, g is the acceleration due to gravity, while n and D are the normal component and the divergence of the mode shape $\boldsymbol{S}$, respectively. The unit normal vector $\boldsymbol{n}$ is defined as pointing into the balloon.

The pneumatic stiffness and damping K_p and R_p in (6) are functions of the turbine coefficient as well as the air volumes. To derive these coefficients, the following steps were taken. First, the volume amplitude v_c was expressed in terms of the unknown displacement amplitude $\xi=-iU/\omega$ and the normal component n of the assumed mode shape

$$v_\text{c}=-\xi\iint_{S_\text{s}} n\,\mathrm{d}S,\qquad(10)$$

where the integral was taken over the mean surface of the balloon. Then, the dynamic pneumatic force on the balloon was expressed to first order as

$$F_\text{p}=-\iint_{S_\text{s}} p_\text{c}n\mathrm{d}S-P\xi\iint_{S_\text{s}} nD\,\mathrm{d}S.\qquad(11)$$

In accordance with the form of the equation of motion (6), the pneumatic stiffness and damping coefficients were thus given as

$$K_\text{p}=\text{Re}\{Ev_\text{c}^2\}+Pv_\text{p}\qquad(12)$$

$$R_\text{p}=\frac{1}{\omega}\text{Im}\{Ev_\text{c}^2\},\qquad(13)$$

with E as defined in (3) and v_c and v_p defined as

$$v_\text{c}=\iint_{S_\text{s}} n\mathrm{d}S\qquad(14)$$

$$v_\text{p}=\iint_{S_\text{s}} nD\mathrm{d}S.\qquad(15)$$

3.2 Present approach

In the present approach, the tendons are discretised into a number of small elements as in the static calculations. The aim is to solve for the displacements (radial and vertical) of each element at its midpoint without making any a priori assumptions on how each element would move, except that the length between any two neighbouring midpoints must not change, consistent with our assumption that the tendons are inextensible.

The tendons are assumed to oscillate harmonically about the mean or static position, so any time-dependent quantity $y(t)$ can be written as $\text{Re}(Y+y\text{e}^{i\omega t})$, where Y is the mean and y is a complex amplitude of the time-dependent part. The approach consists of expanding the static equations of the tendons (2) and (1) to include the time-dependent parts, and then subtracting the static equations from the expanded equations, while keeping only terms up to the first order. The resulting dynamic equations for each tendon element can finally be obtained as

$$\begin{aligned}2\pi h(P_i r_i+p_i R_i)&+F_{\text{e}i}+F_{\text{r}i}=T(a_{i-1}-a_i)-\\&\frac{A_{i-1}-A_i}{\sin A_N}(Ta_N\cos A_N+\pi R_{N+1}^2 p_\text{c}),\end{aligned}\qquad(16)$$

where use has also been made of the bottom boundary condition, which requires that the pulling-down force on the base must be equal to the net upward force on the balloon. Here, we have defined P_i and R_i as the mean pressure and radius at the midpoint of element i, and A_{i-1} and A_i as the mean angles at the ends of element i. The pressure amplitude p_i is equal to p_c if midpoint i is above water, or $p_\text{c}+\rho gz_i$ if it is underwater. Furthermore, $F_{\text{e}i}$ and $F_{\text{r}i}$ are the wave excitation force and the radiation force on element i, while r_i and a_i are the complex amplitudes of the radial and angular displacements, respectively. The radiation force $F_{\text{r}i}$, as usual, can be expressed in terms of the added mass and radiation damping. These, as well as the wave excitation force $F_{\text{e}i}$, which are acting in the direction normal to element i, may be obtained using a 3D panel method [10] by specifying modes associated with the normal displacement of each element of the tendons. The panel models used in the computations are shown in Fig. 6. Equation (16), which pertains to a bottom-fixed balloon, are a special form of the more general equations pertaining to a heaving, floating balloon which is treated in [12].

The pressure amplitude in the balloon p_c is related to the volume amplitude v_c through (3). The volume amplitude v_c can further be expressed in terms of the radial and vertical displacements r_i and z_i of the element midpoints. In addition, the condition that the tendons are inextensible gives a relationship between r_i and z_i. Equation (16) can therefore be formulated in terms of only the radial displacements r_i as the unknowns. The final N independent equations can be written in matrix form and solved using standard methods. Further details are given in [12].

3.3 Comparison of results

Fig. 7 shows the power absorption performance of the bottom-mounted balloons for the cases specified in Table 1. The result is presented in terms of the absorption widths as well as the mean absorbed power per incident wave amplitude squared.

Both the previous and present approaches predict a broad-banded power absorption, but it is clear from Fig. 7 that the previous method largely overestimated the absorbed power. With the present method, the highest absorption is attained by the balloon in case b, but the maximum absorption width with a chamber volume of 2000 m^3 is only about 1.3 m, which is about 12% with respect to the waterplane diameter. As with the previous method, increasing the chamber volume also increases the
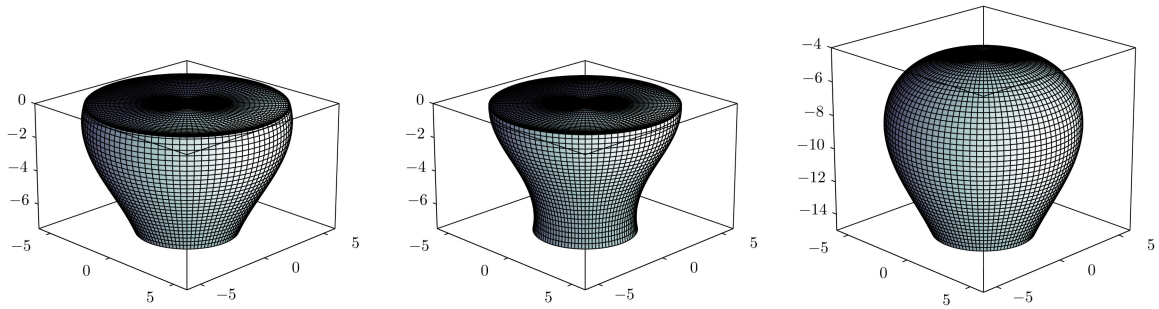
Fig. 6 *Left to right: panel models of the balloon for cases a–c. Axes units are in metres. The interior mean water surface for the surface-piercing cases a and b is discretised as well for the purpose of removing irregular frequency effects*
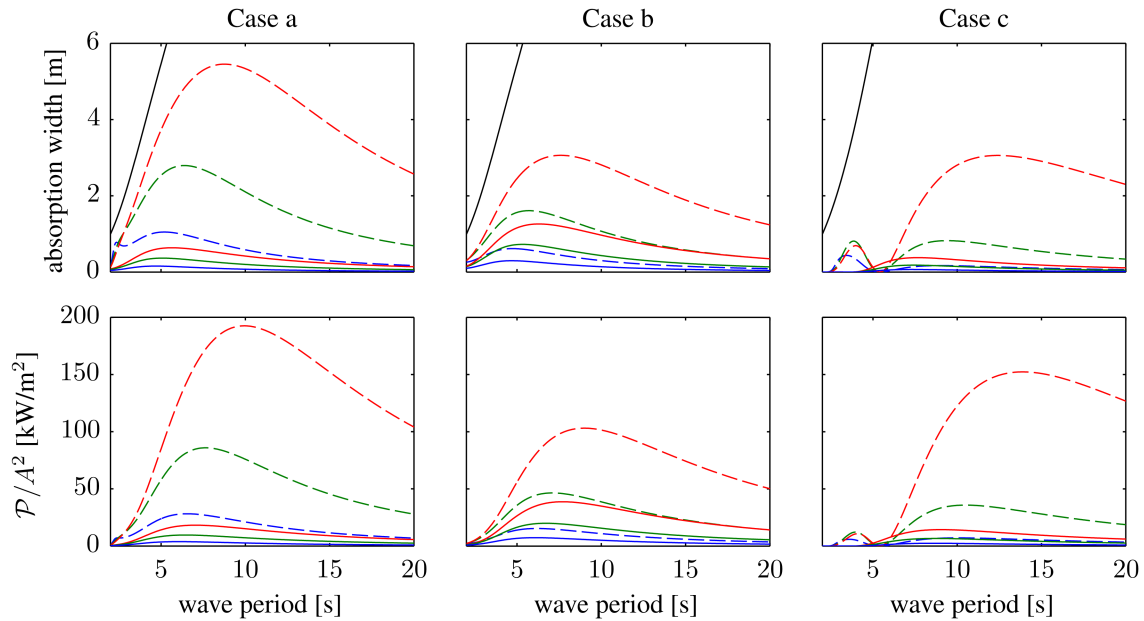

Fig. 7 *Absorption widths and mean absorbed power per incident wave amplitude squared, for cases a–c and different chamber volumes: 500, 1000, and 2000 m³. Solid lines are obtained with the present method, dashed lines with the previous method. The absorbed power increases with larger chamber volume. For the absorption widths, the theoretical maximum λ/2π for point absorbers is also shown as the monotonically increasing solid line. All results are obtained with turbine coefficient C = 0.012 ms*

absorbed power, but at a decreasing rate, such that the maximum absorption width for case b is only slightly above 2 m (or 20% relative to the waterplane diameter) even when very large chamber volumes are used.

The higher power absorption of the balloon in case b compared with a and b seems to agree with the fact that the change in volume around the mean pressure is greater for the balloon in case b than for the balloons in cases a and c (see Fig. 5*b*).

For case c, the present method also predicts a cancellation period at which the absorbed power is zero and below which very little power is absorbed by the balloon. In [5], an explanation behind this cancellation has been suggested. Such cancellation is not uncommon in wave–body interactions and in the present case has to do with the fact that the balloon is completely submerged. As the balloon expands, its lower part deforms normally outward, but its upper part deforms normally inward (compare, for example, profiles a and b of Fig. 4*b*). It is reasonable to expect that there is a particular period, which is dependent on the mean geometry of the balloon, where the waves radiated by the upper and lower parts cancel out. This means that no waves will be radiated by the balloon at this period, and since wave absorption requires wave radiation, no power is absorbed at the same period.

Looking at Fig. 8, we can see a correlation between the power absorbed by the balloon and its volume amplitude. The volume amplitude of the balloon is found to be relatively small, and to absorb an appreciable level of power the balloon has to respond with greater amplitudes, which seems possible for this bottom-mounted balloon only if the incident wave amplitudes are higher. In addition, the pressure amplitudes are found to be only about half

the incident wave amplitude, in contrast to the case of a heaving balloon, where the pressure amplitudes in the balloon can be up to twice the incident wave amplitude [12].

With the previous method, the smallest amplitudes of the displacement of the bag top are obtained for case b, but the opposite is true with the present method, where the amplitudes are the largest for case b. This clearly indicates that the deformations of the balloon predicted using the two approaches are quite different. Indeed, we see from Fig. 9 that the actual deformations of the balloon obtained using the present method differ from the mode shape used in the previous method. The difference is especially greater above the waterline.

4 Concluding remarks

The possibility of absorbing energy from the waves using a bottom-mounted balloon has been investigated. Compared with the wave power incident on the balloon, the power absorbed by the balloon is found to be very small. The latest results have been obtained using a method which puts no restrictions on the way the tendons move, apart from ensuring that the length of the tendon must not change. The previous method, on the other hand, prescribes the way the tendons move, and is found to overestimate the absorbed power quite substantially. The inadequacy of the previous method has been highlighted by comparing the prescribed mode shape and the actual deformations predicted by the present method.

This study suggests that it might be better for such balloon as considered here to be floating and heaving in the water rather than
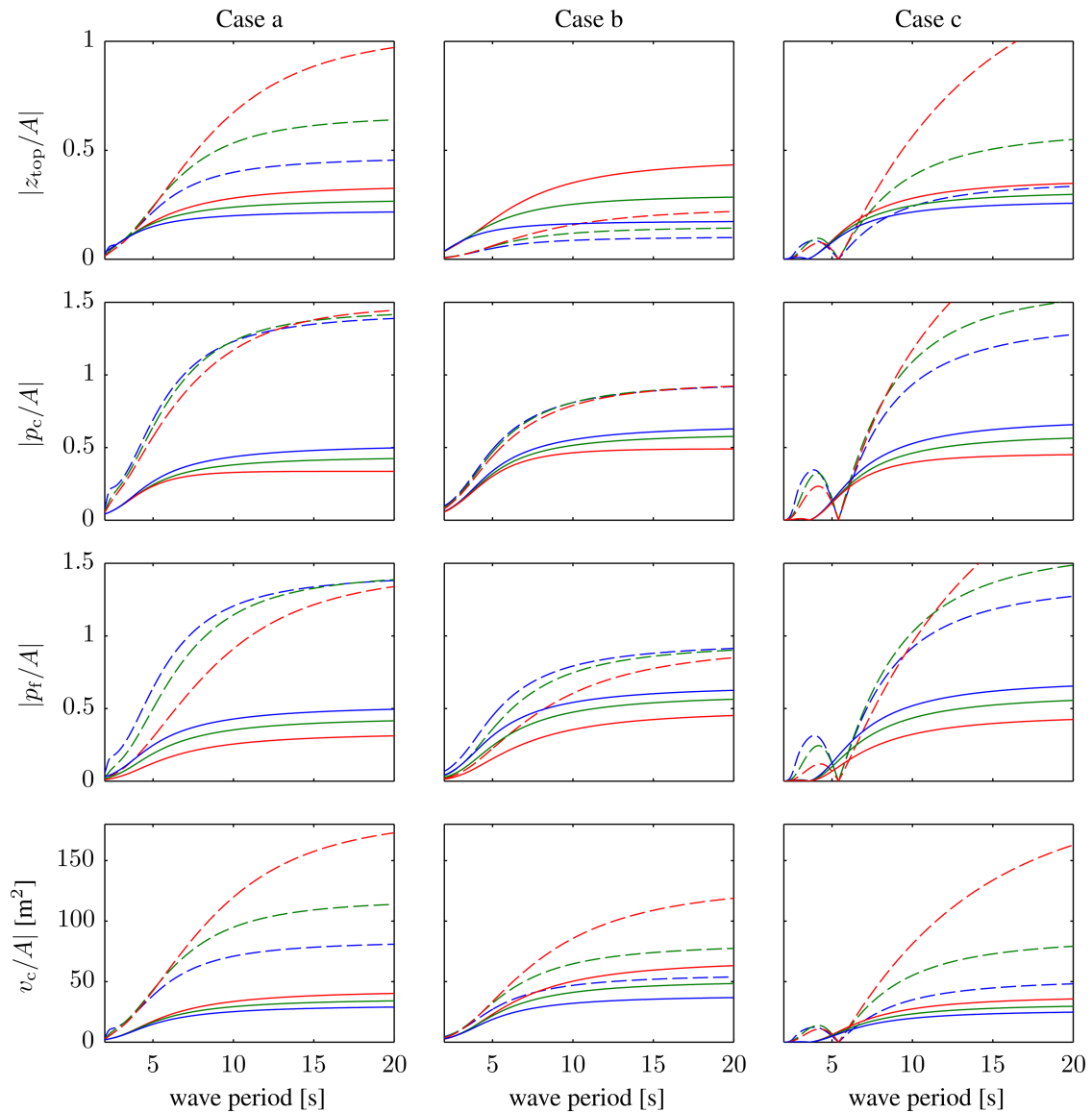
Fig. 8 *Normalised displacement amplitudes of the top of the balloon, and of the pressures in the balloon and in the chamber, and volume amplitudes of the balloon per wave amplitude, corresponding to Fig. 7. The top displacement and the volume amplitude of the balloon increase with larger chamber volume. The pressure amplitudes in the balloon and in the chamber decrease with larger chamber volume, except for case c, where the previous method predicted increasing pressure amplitudes at larger periods*
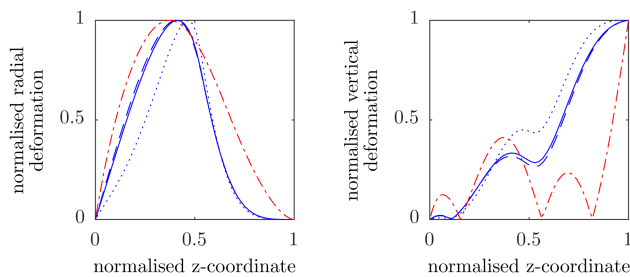

Fig. 9 *Normalised radial and vertical deformations of the balloon in case b, at 8 s (solid), 3 s (dotted), and 15 s (dashed). The radial and vertical components of the mode shape used in the previous method are drawn in dash-dotted lines*

fixed to the sea bed. It would also be interesting to see if two bottom-mounted balloons exchanging air between them (Fig. 2b) could have better performance than a single balloon exchanging air with a constant-volume chamber as treated here. In addition, other geometries radically different from those considered here, such as a completely submerged balloon with a very large diameter at the base, deserve a further study.

6 References

[1] Mei, C.C.: 'Power extraction from water waves', *J. Ship Res.*, 1976, **20**, (2), pp. 63–66

[2] Evans, D.V.: 'A theory for wave power absorption by oscillating bodies', *J. Fluid Mech.*, 1976, **77**, (1), pp. 1–25

[3] Budal, K., Falnes, J.: 'A resonant point absorber of ocean-wave power', *Nature*, 1975, **256**, pp. 478–479, with Corrigendum in Nature, vol. 257, p. 626, 1975

[4] Kurniawan, A., Greaves, D., Chaplin, J.: 'Wave energy devices with compressible volumes', *Proc. R. Soc. Lond. A*, 2014, **470**, (2172)

[5] Kurniawan, A., Greaves, D.: 'Broad-banded wave power absorption with submerged balloons'. Proc. of the Second Offshore Energy and Storage Symp., Edinburgh, UK, 2015

[6] Pimm, A.J., Garvey, S.D., de Jong, M.: 'Design and testing of energy bags for underwater compressed air energy storage', *Energy*, 2014, **66**, pp. 496–508

[7] Uwatoko, T., Ijima, T., Ushifusa, Y., *et al.*: 'Wave interception by sea-balloon breakwater', *Coast. Eng. Proc.*, 1986, **1**, (20), pp. 2353–2367

[8] Taylor, G.I.: 'On the shapes of parachutes'. in Batchelor, G.K. (ED.): '*The scientific papers of G. I. Taylor*' (Cambridge University Press, Cambridge, 1963), pp. 26–37 (Original work published 1919)

[9]   Chaplin, J., Farley, F., Greaves, D.*, et al.*: 'Numerical and experimental investigation of wave energy devices with inflated bags'. Proc. 11th European Wave and Tidal Energy Conf., Nantes, France, 2015

[10]   WAMIT. WAMIT, Inc., Chestnut Hill, MA, 2015. Version 7.1

[11]   Newman, J.N.: 'Wave effects on deformable bodies', *Appl. Ocean Res.*, 1994, **16**, pp. 47–59

[12]   Kurniawan, A., Chaplin, J.R., Greaves, D.M.*, et al.*: 'Wave energy absorption by a floating air bag', submitted

IET Renew. Power Gener., 2016, Vol. 10 Iss. 10, pp. 1461-1467

1467